# STAR FORMATION IN THE MAGELLANIC IRREGULAR GALAXY NGC 4449

Harley A. Thronson, Jr.,[1] Deidre A. Hunter,[2] C. M. Telesco[3,5]

and

D. A. Harper[4] and R. Decher[3,5]

Received: _____

[1]Wyoming Infrared Observatory, University of Wyoming

[2]Department of Terrestrial Magnetism, Carnegie Institution of Washington

[3]Space Science Laboratory, NASA Marshall Space Flight Center

[4]Yerkes Obsevatory, University of Chicago

[5]Visiting Astronomer, NASA Infrared Telescope Facility, which is operated by the University of Hawaii under contract to NASA.

## ABSTRACT

New near- and far-infrared mapping and J = 1 → 0 CO spectroscopy of the Magellanic irregular galaxy NGC 4449 are presented. We find that the brighter 150 μm emission is concentrated along the bright central visual ridge of the galaxy, although there is lower-intensity extended emission throughout the visible extent of the object. The maximum far-infrared emission is coincident, within the uncertainties, with the visual and near-infrared emission maxima, which we identify as the galactic nucleus. We estimate that the infrared luminosity of the central 1 kpc diameter region in NGC 4449 is comparable to that for a similar-sized region at the center of the Milky Way. A large fraction of the 150 μm emission may arise from warm dust distributed throughout the galaxy and heated by the diffuse radiation field. Active star formation follows the near-infrared emission in part of the galaxy, but no coincidence is found in another region. The distribution of K-band light is not similar to that found for galactic bars, as usually defined. The J = 1 → 0 CO line emission has a maximum near the apparent center of the galaxy, although an offset of up to ∿1 kpc is also possible.



Subject headings: galaxies: general --- galaxies: individual (NGC 4449) -- stars: formation.

# I. INTRODUCTION

Increasing attention is being paid to the large Magellanic irregular galaxies as it has become apparent that they may be the most abundant, as well as the most efficient, of the star-forming galaxies (e.g., Gallagher, Hunter, and Tutukov 1984; Hunter, Gallagher, and Rautenkranz 1982; Hunter et al. 1986; Thronson and Telesco 1986; see also the reviews by Gallagher and Hunter 1984, 1986). At the same time, because of their lack of pronounced spiral structure, the Magellanic irregulars provide a perspective on the large-scale properties of star formation that complements studies of the giant spirals.

Among the best known of the Magellanic irregular galaxies is NGC 4449, a high-surface brightness object that has been extensively studied at visual (Hunter, Gallagher, and Rautenkranz; Gallagher, Hunter, and Tutukov; Bothun 1986), thermal infrared (Hunter et al. 1986), and millimeter wavelengths (Tacconi and Young 1985). These authors found that the galaxy is sustaining a high rate of star formation, and has apparently maintained this rate for at least $\sim 10^9$ years despite the presence of only moderate amounts of molecular material. The galaxy has a large amount of atomic gas which may be participating directly in forming stars.

In this paper we present millimeter-wave and near- and far-infrared observations of NGC 4449 which we use to estimate the rate, efficiency, and location of star formation as well as the abundance of molecular gas.

## II. OBSERVATIONS AND REDUCTION

### a) The Airborne Observations

NGC 4449 was observed using the 0.9 m telescope aboard NASA's Kuiper Airborne Observatory (KAO) during May 1985. The detector system was a 32-element array of Ge(Ga) bolometer detectors, each mounted behind a light-collecting cone (Harper et al. 1976). At the Nasmyth focus of the telescope, the angular diameter (FWHM) of each circular pixel was 45" ± 5" and the center-to-center separation was 50". The absolute positional accuracy of these far-infrared observations is estimated to be ±20" (±1σ rms) and includes the effect of personal judgement in choosing the locations of contours in regions of the map that were spatially undersampled. For the observations that we report here, we used a broadband filter with half-power points at $\lambda$ = 130 μm and $\lambda$ = 270 μm. For a wide range of far-infrared spectra, the effective wavelength was within ±10 μm of $\lambda$ = 150 μm. During the course of the observations, the reference beam spacing was 3!8 and oriented with an average position angle of 160° (measured from north through east). During the entire period of observation of NGC 4449, the object rotated only about 10°, which has no effect on the reduction of our data. Flux density calibration was accomplished by observing M82 using data from Telesco and Harper (1980) and D. Harper (unpublished). We estimate a ±20% (1σ rms) systematic uncertainty in this calibration.

Our far-infrared results are presented in Figures 1, 2, and 3 as a 150 μm map of NGC 4449, a diagram showing the positions at which data were taken, and the infrared spectrum of the object. The observed flux

densities are normalized to a peak value of 100, which results in the highest drawn contour being equal to 80. In Figure 1 the outermost, dashed contour corresponds to a signal-to-noise ratio of 2. The integration time was 6 minutes at each of the positions in Figure 2.

The total infrared spectrum for the source (Figure 3) rises steeply from 10 μm through 150 μm. From the 100 μm and 150 μm data points, we estimate a characteristic dust temperature of $T_d$ = 25 K. This assumes that the thermal spectrum is of the form $F_\nu \propto \nu B_\nu(T_d)$, appropriate for dust emission from individual star-forming regions in the Milky Way (Thronson and Harper 1979; Rowan-Robinson 1980; Hildebrand 1983). A spectrum of the form $\nu B_\nu$(25 K) is drawn in the figure. It is worth emphasizing that emitting regions with a broad range of physical conditions are contributing to the observed energy distribution. This heterogeneity is partly manifested by the excess emission shortward of 100 μm above that expected for the 25 K emission. It is clear that a range of dust temperatures is present.

Integrating under the $\nu B_\nu$(25 K) curve in Figure 3 we find $L_{IR} = 2.5 \times 10^9 L_\odot$ for the entire galaxy at a distance of 5.4 Mpc using $H_o$ = 50 km $s^{-1}$ $Mpc^{-1}$ (Hunter, Gallagher, and Rautenkranz 1982). Where necessary, parameters calculated by other workers who adopted a different distance will be adjusted accordingly. Integrating under the observed points (10 μm - 150 μm), we find $L_{IR} = 3.2 \times 10^9 L_\odot$, which we adopt as the best estimate of the total far-infrared luminosity. These values are about 50% higher than those calculated by Hunter et al. (1986), primarily because we estimate the total flux over a larger wavelength range.

Adopting a temperature allows the mass of dust in emission at 150 μm to be estimated using the formula and parameters suggested by Hildebrand

(1983), $M_d(M_\odot) \approx 11\ D^2(\mathrm{Mpc})\ F_\nu[\exp(96/T_d)-1]$ where $F_\nu$ is the 150 μm flux density. We calculate $M_d \approx 1.5 \times 10^6\ M_\odot$, which is in good agreement with that calculated by Hunter et al., an agreement that we consider fortuitous because the physical properties of the grains that enter into the calculation are poorly known. Thronson and Mozurkewich (1986) suggest that the total gas mass in a Milky Way star-forming region is 1300 times greater than the mass of dust emitting at about 100 μm, or $M(\mathrm{gas}) \approx 2 \times 10^9\ M_\odot$, in agreement with the 21-cm HI mass determination (Hunter and Gallagher 1985b). In §IIIc we discuss the consequences of there being a large amount of dust in NGC 4449.

### b) The Near-Infrared Observations

We observed the central 80" of NGC 4449 in the near-infrared using the 3 m telescope of the NASA Infrared Telescope Facility (IRTF) on Mauna Kea, Hawaii. We used a single-channel InSb detector with standard near-infrared passband filters. The diameter of the circular beam was 8" and the reference beam spacing was 90", with the line between the signal and the sky-reference position being oriented with P.A. = 135°. This chopper throw placed the reference beam within the Holmberg radius of the galaxy, but judging from the results presented in Figure 4 the contamination from extended emission is much less than a few percent. The photometric standard star was BS 4550 for which we adopted J = 4.91, H = 4.44, and K = 4.38 mag. Observed and calculated parameters are presented in Table 2.

NGC 4449 was mapped only in the K band (2.20 μm). In Figure 5 the K map is shown overlaid on a B image of the galaxy, and subsets of these

data, corresponding to scans along the major and minor axes, are presented in Figure 6. The position of peak 2.2 μm emission (Table 2) is shown as a cross in the 150 μm-Hα map (Figure 1). Within the uncertainties the position of the 2.2 μm peak coincides with the visual nucleus determined by Gallouet, Heidmann, and Dampierre (1973). The position of maximum far-infrared emission is offset from the 2.2 μm peak by an amount comparable to the estimated positional uncertainties.

### c) The Millimeter Wave Observations

During October 1985, NGC 4449 was observed using the 12 m NRAO telescope on Kitt Peak in Arizona.[1] The system was tuned to detect the J = 1 → 0 transition of $^{12}C^{16}O$ (hereafter, CO) at 115 GHz. and we used a cooled Cassegrain Schottky mixer receiver. At this frequency the beamsize of the telescope is 60". The reference position was 10' away in an area found to be devoid of CO emission. The frequency resolution of the observations reported here were 1 MHz (2.6 km $s^{-1}$), but were Hanning-smoothed to $\Delta v$ = 3.7 km $s^{-1}$. Relative calibration was accomplished by the standard NRAO chopper-wheel technique, and an absolute calibration was produced by regularly observing IRC+10°216 for which we took $T_R^*(CO)$ = 6.5 K. Peak antenna temperatures for the calibration objects were repeatable to within 10%. We estimate that the absolute pointing accuracy of the telescope was ±10" (±1σ rms).

[1] The National Radio Astronomy Observatory is operated by Associated Universities, Inc., under contract with the National Science Foundation.

The position of the nucleus (see below) and three outlying positions along the 150 μm ridge were observed, and the results are presented in Table 3 and Figure 7. The northernmost position in the galaxy (the last entry in the table) was observed for only once, and for a relatively short period of time compared to the other points; the values in brackets are therefore less reliable.

## III. ANALYSIS AND DISCUSSION

### a) Far-Infrared Emission

Figure 1 shows that there is a good spatial correlation between the 150 μm emission from dust and the distribution of Hα emission from ionized gas, although this conclusion is limited by the angular resolution of the airborne observations. This correlation between these two tracers of star formation is anticipated from our current understanding about the structure and evolution of regions of star formation in our own galaxy (e.g., Krugel, Cox, and Mezger 1984; Hunter et al. 1986). However, the emission at 150 μm is more extended than the brightest Hα emission, particularly in the direction southeast of the nucleus. The dashed contour in Figure 1 appears roughly circular and covers an area about twice that of the brightest Hα emission. At least 1/3 of the total 150 μm flux density appears to come from regions in the galaxy that show little or no Hα emission in our figure.

This extended, diffuse far-infrared emitting region may contribute significantly to the energy distribution observed at the longest wavelengths

($\lambda \gtrsim 100$ μm). Far-infrared spectra of galaxies generally turn over near 80-100 μm, declining at longer wavelengths (Telesco and Harper 1980, Rickard and Harvey 1984). The energy distribution in Figure 3 shows no evidence for decline at the longest wavelength observed, implying that there is a great deal of far-infrared emission from 20-25 K dust, which would dominate the 150 μm emission.

The 150 μm ridge that extends primarily in declination in Figure 1 appears to be directly associated with particular regions of active star formation, but the outer contours show no clear association with strong Hα emission. It is our interpretation that the more extended 150 μm emission originates in a large amount of cool very extended dust. Star formation may be so energetic within NGC 4449 that ultraviolet and visual radiation escaping the immediate vicinity of the young stars can heat the dust that is distributed throughout the object. The spectral energy distribution of the entire galaxy may be interpreted as the superposition of at least two spatially distinct components: warm dust dominating the emission at $\lambda \lesssim 60$ μm and located in the immediate vicinity of the star-forming clouds, and the cooler dust, with $T_d \lesssim 25$ K, providing the more extended emission.

Radiation originating from a luminous complex of young stars can heat very distant dust grains to 25 K. If R is the distance between a heating source of luminosity $L_*$ and the grains, radiative equilibrium implies

$$T_d(K) \approx 51\left[\frac{0.06}{R(pc)}\right]^{1/3}\left[\frac{L_*(L_\odot)}{10^5 f}\right]^{1/6}, \qquad (1)$$

where the grain absorption efficiency may be written $Q(\lambda) = (50\ \mu m/\lambda)^2 f$, a relation applicable to the longer far-infrared wavelengths (e.g., Hildebrand 1983). Equation (1) was taken from Scoville and Kwan (1976), but the resultant dust temperatures agree with calculations made a number of different ways. We take $f = 0.01$ (Hildebrand 1983), and we assume that half the observed infrared luminosity (Table 1) is free to heat the extended material. For a typical distance of 1' (1.6 kpc) of the grains from the energetic center of NGC 4449 (Figure 1), equation (1) implies $T_d = 19$ K. Since the object's spectrum is still rising at $\lambda = 150\ \mu m$, this value for $T_d$ is reasonable. Thus, we conclude that significant emission from an extended distribution of dust with $T_d \approx 25$ K may be common in objects such as NGC 4449.

### b) The Nucleus of NGC 4449

NGC 4449 appears to possess a distinct nucleus, a small region toward the center of the galaxy that is substantially brighter than its surroundings (e.g., Bothun 1986). A goal of this program was to more thoroughly characterize the nucleus of this irregular galaxy for comparison with our far-infrared and millimeter-wave CO observations. Photospheric emission from red giant stars usually dominates the near-infrared emission from galaxies (Frogel et al. 1978; Persson et al. 1983; Telesco, Decher, and Gatley 1985). These stars are tracers of the old stellar mass. In Figure 1, a cross is shown at the position of peak 2.2 μm emission. Within the uncertainties of the observation (±3"), the K-band (2 μm) peak is identical to the visual emission maximum (Gallouet, Heidmann, and Dampierre 1973). The

JHK colors of this 2.2 μm peak are similar to those of the nuclei of ellipticals and spirals (Frogel et al.) in which the infrared radiation is dominated by giants.

Figure 1 indicates that the far-infrared maximum and the nucleus of NGC 4449 roughly coincide, and therefore star formation is most pronounced near the position of which the mass of old stars is greatest (conventionally referred to as the "nucleus"). Despite this, 85% of the total 150 μm emission arises from the lower surface brightness regions outside the 45" KAO beam centered on the nucleus. Although the association between the far-infrared peak and the nucleus may be close, the positional uncertainty (30") in the far-infrared map can accomodate a positional offset between the two.

The far-infrared luminosity contained within the 45"-diameter (1.2 kpc) beam at the peak of NGC 4449 is $\sim 4 \times 10^8$ $L_\odot$ or about 1/8 that of the whole galaxy. On the basis of available data, it is difficult to estimate the total luminosity of the central few hundred parsecs of the Milky Way, but $L_{IR} = 5 - 10 \times 10^8$ $L_\odot$ is a fair estimate (Gatley et al. 1978, Gautier et al. 1984, Odenwald and Fazio 1984, Campbell et al. 1985). Therefore, within a factor of three, the far-infrared nuclear emission from the central regions of NGC 4449 is equal to that from the same region in the Milky Way. If the mass-to-luminosity ratio of a young stellar cluster is $4 \times 10^{-3}$ $M_\odot$ $L_\odot^{-1}$ (Thronson and Telesco 1986), then the mass of young stars in the center of NGC 4449 is $\sim 2 \times 10^6$ $M_\odot$.

Bothun (1986) identified the nucleus as a probably large OB association with a B luminosity of $5 \times 10^6$ $L_\odot$ at our adopted distance of 5.4 Mpc. This object(s) thus makes a negligible contribution to the heating of the dust that is included in the KAO beam centered on this position.

## c) The CO Emission

Detection of the $J = 1 \rightarrow 0$ CO emission from NGC 4449 permits an estimate to be made of the molecular mass in the core of the galaxy.

Tacconi and Young (1985) also studied the CO emission from this galaxy, using the FCRAO 14 m telescope which has a half-power beam width of 50". The nucleus was the one position in the galaxy that was observed by both groups; within the uncertainties, the observed line strengths there are in agreement. In addition, both groups find that the CO line strengths about 1' south of the nucleus are comparable to the nuclear position. Wtihin a factor of two, three positions in this galaxy each separated by 1' show approximately the same CO line strength despite significant differences in apparent H$\alpha$ brightness and far-infrared emission (Figure 1).

The 150 $\mu$m emission optical depth may be estimated from $F_\nu = \Omega B_\nu(T_d)(1 - e^{-\tau})$, where $\Omega$ is the beam solid angle and $F_\nu$ is the observed flux density. Following the discussion in §IIa, we adopt a characteristic temperature $T_d = 25$ K and calculate the optical depth for the four positions for which we obtained reliable CO spectra. The results are presented in Table 3. For the three reliable CO spectra, we obtain $I_{CO}(K - km\ s^{-1}) = 1.6 \times 10^3\ \tau[150\ \mu m]$. This relates $\tau[150\ \mu m]$ to the $H_2$ column density through $I_{CO}$.

Young and Scoville (1982) derived a relation to estimate the line-of-sight $H_2$ mass and column density for a galaxy, using the observed CO luminosity:

$$N(H_2)\ cm^{-2} \approx 4 \times 10^{20}\ I_{CO}\ K - km\ s^{-1},$$

$$\text{or,}\quad M(H_2)\ M_\odot \approx 6.5 \times 10^{6}\ I_{CO}\ K - km\ s^{-1}, \qquad (2)$$

for the beam size of the NRAO telescope at the distance of NGC 4449. From the three reliable detections of CO emission (Table 3), we estimate the total $H_2$ mass to be at least $1.6 \times 10^7\ M_\odot$. At the position of the nucleus, where we estimate that there is $2 \times 10^6\ M_\odot$ of young stars (§IIIb), equation (2) and the results in Table 3 indicate that the molecular mass is $M(H_2) \approx 7 \times 10^6\ M_\odot$. Star formation may be proceeding within this galaxy with a high efficiency.

### d) The Near-Infrared Structure

As noted above, we adopt the view that the older stars dominate the 2 μm light and that they trace the dominant underlying stellar mass distribution. The limited multi-color photometry that we obtained are consistent with this assumption. Both the nuclear colors and those obtained along the major axis are comparable to those of the old stellar populations in globular clusters, elliptical galaxies, and the nuclei of most spirals (e.g., Frogel et al. 1978, Persson et al. 1983). Slight variations of JHK colors with positions are likely to be due to a contribution to the near-infrared light from the photospheres of blue stars or bremsstrahlung emission from H II regions.

Southwest of the nucleus the dominant star formation evident in the far-infrared and the Hα and blue photographs generally follows the

elongated 2 μm distribution (Figure 5). However, this correlation is not evident north of the nucleus. In this direction the far-infrared emission appears to generally follow the bright Hα emission (Figure 1), but neither component is coincident with the 2 μm "bar". We conclude that while there may be a trend for star formation to occur along the near-infrared "bar", significant star-forming complexes without an obvious relationship to the bar are evident.

In the scans at K along the major and the minor axes (Figure 6), the near-infrared nucleus stands out almost as a point source superimposed on a broader emission. Along the major axis we have fit the function

$$F(mJy) = 11.5 \times (1.046)^{-r} \qquad (3)$$

where the radius from the central point source, r, is in arcseconds. To convert magnitudes to flux densities, we took $F_0 = 632$ Jy for K = 0. Bothun (1986) determined the B and R light profiles along the galaxy's major axis and also found good agreement with an exponential fall-off with radial distance. He found a scale length of about 30" in both visual colors, in agreement with that which we find for K for the major axis in NGC 4449.

The fact that there is a sharp decrease in K brightness in all directions away from the central maximum means that the bar-like feature that we have mapped at near-infrared wavelengths is not a structure similar to that found in barred spirals. Kormendy (1982) described a "true" bar as a structure with almost constant surface brightness along its major axis interior to a sharp outer edge and following a $r^{1/4}$ law along

the minor axis. As is evident from Figure 6 a $r^{1/4}$ law does provide a reasonable fit to the minor axis brightness distribution, but clearly not to that for the major axis. Despite this fit and the fact that there is some variation in the characteristics among well-recognized bars, NGC 4449 does not appear to possess a bar as is usually defined.

e) The Star Formation Rate

Star formation rates can be determined for objects for which some measure of the number of young stars is available. We use the parameters and assumptions of Thronson and Telesco (1986). They assume, as do many others, that because of the large visual and ultraviolet absorption efficiency of grains, the far-infrared luminosity measures the total luminosity of all newly formed stars. They further assume that the radiation field due to the older stellar population does not contribute to the heating of the dust. These young stars are taken to form with a mass distribution given by the Miller-Scalo function over the mass range $0.1 \rightarrow 100\ M_\odot$. We derive a "current" star formation rate (i.e., averaged over the past $2 \times 10^6$ yrs; Thronson and Telesco 1986):

$$\dot{M}_{IR}(M_\odot\ yr^{-1}) = 2.2 \times 10^{-9}\ L_{IR}\ (L_\odot), \qquad (4)$$

or $\dot{M} = 7\ M_\odot\ yr^{-1}$ for all of NGC 4449. This rate would be about a factor of 2.5 lower if only O, B, and A stars form. Hunter et al. (1986) calculated a value for $\dot{M}$ of about $1\ M_\odot\ yr^{-1}$ for NGC 4449. Their value differs from ours due in part to a lower estimated total luminosity and in part due to

their adoption of a Salpeter mass function, which produces a smaller mass-per-luminosity ratio than the Miller-Scalo function.

Hunter et al. also calculated a star formation rate from the Hα luminosity and found it to be in good agreement with that which they calculated from the infrared luminosity. This agreement supports the view that the infrared-emitting dust is heated by newly-formed stars, the same stars that ionize the gas. The dust is not significantly heated by the older stellar population.

Gallagher, Hunter, and Tutukov (1984), Hunter et al., and Thronson and Telesco (1986) discuss using the blue luminosity of a galaxy to estimate the star formation rate averaged over the past several hundred million years or so. Using an assumed initial mass function $\psi(M)$, the recent stellar mass formation rate can be estimated from

$$M_B \approx [\int \psi(M) M dM / \int \psi(M) \ell_B(M) t(M) dM] L_B, \qquad (5)$$

where $\ell_B(M)$ is the luminosity in the blue band of a star of mass M and t(M) is its main sequence lifetime or $10^9$ years, whichever is shorter. These assumptions give

$$\dot{M}_B(M_\odot\ yr^{-1}) = 5.1 \times 10^{-9}\ L_B\ (L_\odot) \qquad (6)$$

for a Miller-Scalo initial mass function. For a Salpeter function the coefficient in the equation is $6.5 \times 10^{-9}$. The blue magnitude of the galaxy is $B^\circ_T = 9.95$ (de Vaucouleurs, de Vaucouleurs, and Corwin 1976), or $L_B = 6.8 \times 10^8\ L_\odot$. Thus, the averaged star formation rate for the

past $10^9$ years is at least 3 $M_\odot$ $yr^{-1}$, similar to the rate found from the infrared data. This value is about a factor of 7 greater than that calculated by Gallagher, Hunter, and Tutukov (1984).

The total gas mass in NGC 4449 is $\sim 10^{10}$ $M_\odot$ (Hunter and Gallagher 1985c, Tacconi and Young 1985), so that the average star formation rate can be maintained for at least a few times $10^9$ years.

## IV. SUMMARY

The essential points of our study of the Magellanic irregular galaxy NGC 4449 may be summarized as follows.

1. Far-infrared emission, characterized by a dust temperature of 25 K, is found throughout the visual extent of the galaxy. This emission is especially concentrated along a central ridge, coincident with the brighter visual-wavelength emission. Extremely active star formation can sustain the large-scale 150 μm emission.

2. The infrared luminosity -- 3.2 x $10^9$ $L_\odot$ -- is interpreted as the result of a current star formation rate of about 7 $M_\odot$ $yr^{-1}$. The central 1 kpc of NGC 4449 has an infrared luminosity comparable to that of the similar-size region in our own galaxy.

3. The total amount of gaseous material in NGC 4449, as calculated from the far-infrared flux, is about 2 x $10^9$ $M_\odot$, in agreement with that found from 21 cm line observations.

4. We find a coincidence in position between the visual, near- and far-infrared emission maxima. The near-infrared colors of this object are similar to those found for the nuclei of spiral and elliptical galaxies, and imply that the emission maxima approximately coincide with the maxima of the stellar mass distribution.

5. The central ridge of active star formation appears to follow the distribution of older stars southwest of the nucleus. However, on the opposite side of the nucleus, toward the northeast, there is no correspondence between the apparent location of the old stars and of the most active star formation.

6. The prominent visual and near-infrared ridge in the NGC 4449 does not meet the usual criteria for a galaxian bar. In particular, the brightness along the major axis falls off with radius more rapidly than for a "true" bar.

7. Based upon a comparison between the infrared and the blue luminosity, the galaxy is presently undergoing a period of star formation at a rate roughly equal to that averaged over the past $10^9$ years. The available atomic and molecular gas may be sufficient to sustain this rate for a few times $10^9$ years.

We appreciate the fine support of the NASA Ames Medium Altitude Missions Branch and the Tucson NRAO staff. At the 12 m site, Messrs. Grote Reber, John Weaver, and Cal Sparks assisted in the time-consuming system changes that took place during our observations. We appreciate the useful comments of J. Gallagher. Jackie Davidson at Yerkes Observatory assisted with the analysis of the far-infrared data. Most of this work was supported by NASA Grant NAG 2-134.

R. Decher and C. M. Telesco, ES-63, Space Science Lab, NASA Marshall Space Flight Center, Huntsville, AL 35812.

D. A. Harper, P.O. Box 258, Yerkes Observatory, Williams Bay, WI 53191.

D. A. Hunter, Dept. of Terrestrial Magnetism, 5241 Broad Branch Rd., N.W., Washington, D.C. 20015.

H. A. Thronson, Dept. of Physics and Astronomy, University of Wyoming, Laramie, WY 82071.

TABLE 1

Far-Infrared Flux Densities

NGC 4449

| | | |
|---|---|---|
| Integrated (Jy) | 12 μm | 2.1 ± 0.2[a] |
| | 25 μm | 4.7 ± 0.5[a] |
| | 60 μm | 36 ± 3[a] |
| | 100 μm | 73 ± 8[a] |
| | 150 μm | 100 ± 20[b] |

Derived Quantities

| | |
|---|---|
| Luminosity (10-150 μm)[c] | $32 \times 10^8 L_\odot$ |
| Dust mass[d] | $1.5 \times 10^6 M_\odot$ |
| Characteristic dust temperature[e] | 25 K |
| Current star formation rate | $7 M_\odot\ yr^{-1}$ |

Notes:

[a] IRAS data (Hunter et al. 1986)

[b] KAO data (this work)

[c] distance = 5.4 Mpc

[d] See §IIIc

[e] From 150 μm and 100 μm data

TABLE 2

Near-Infrared Magnitudes

NGC 4449

| | | |
|---|---|---|
| Peak (8" beam) | J = 12.08 | (1.25 μm) |
| | H = 11.37 | (1.65 μm) |
| | K = 11.15 | (2.20 μm) |

K Peak Position and galactic nucleus

$\alpha(1950) = 12^h\ 25^m\ 46^s.8$

$\delta(1950) = 44°\ 22'\ 20"$

TABLE 3

Millimeter-wave Observations

| α(1950) | δ(1950) | $\int T_R^* dv$ [K-km $s^{-1}$] | $V_{LSR}$[km $s^{-1}$] | ΔV[km $s^{-1}$] | τ[$10^{-4}$][c] |
|---|---|---|---|---|---|
| $12^h\ 25^m\ 45^s.0$ | 44° 21' 8" | 0.89 ± 0.24 | 211 | 44 | 3 |
| 12 25 46.8 | 44 22 6[a] | 1.02 ± 0.15 | 223 | 44 | 11 |
| 12 25 48.6 | 44 23 4 | 0.59 ± 0.13 | 224 | 50 | 6 |
| 12 25 50.4 | 44 24 2 | [2.4 ± 0.5][b] | [230][b] | [110][b] | 4 |

Uncertainties on integrated line strength are ±1σ rms.

[a]Nuclear position

[b]Extremely uncertain values; see §IIc.

[c]150 μm emission optical depth; see §IIIc.

## REFERENCES


Bothun, G. D. 1986, A. J., in press.

Campbell, M. F. et al. 1985, Adv. Space Res., 5, 3.

de Vaucouleurs, G., de Vaucouleurs, A., and Corwin, H. 1976, Second Reference Catalogue of Bright Galaxies (Austin: University of Texas Press).

Elmegreen, B. G., Elmegreen, D. M., and Morris, M. 1980, Ap. J., 240, 455.

Frogel, J. A., Persson, S. E., Aaronson, M., and Matthews, K. 1978, Ap. J., 220, 75.

Gallagher, J. S., and Hunter, D. A. 1984, Ann. Rev. Astr. Ap., 22, 37.

Gallagher, J. S., and Hunter, D. A. 1986, Pub. A.S.P., 98, 5.

Gallagher, J. S., Hunter, D. A., and Tutukov, A. V. 1984, Ap. J., 284, 544.

Gallouet, L., Heidmann, N., and Dampierre, F. 1973, Astr. Ap. Suppl., 12, 89.

Gautier, T. N. et al. 1984, Ap. J. (Letters), 278, L57.

Harper, D. A., Hildebrand, R. H., Stiening, R., and Winston, R. 1976, Appl. Optics, 15, 53.

Harvey, P. M., Campbell, M. F., and Hoffmann, W. F. 1977, Ap. J., 211, 786.

Hildebrand, R. 1983, Q.J.R.A.S., 24, 267.

Hunter, D. A. 1982, Ap. J., 260, 81.

Hunter, D. A., and Gallagher, J. S. 1985a, A. J., 90, 1457.

Hunter, D. A., and Gallagher, J. S. 1985b, A. J., in press.

Hunter, D. A., Gallagher, J. S., and Rautenkranz, D. 1982, Ap. J. Suppl., 49, 53.

Hunter, D. A., Gillett, F. C., Gallagher, J. S., Rice, W. L., and Low, F. J. 1986, Ap. J., in press.

Kormendy, J. 1977a, Ap. J., 214, 359.

Kormendy, J. 1977b, Ap. J., 218, 333.

Kutner, M. L., and Leung, C. M. 1985, Ap. J., 291, 188.

Krugel, E., Cox, P., and Mezger, P. G. 1984, Airborne Astronomy Symposium, NASA Conference Publication 2353, eds. H. Thronson and E. F. Erickson (Moffett Field, CA: NASA Ames Research Center), p. 300.

Persson, S. E., Aaronson, M., Cohen, J. G., Forgel, J. A., and Matthews, K. 1983, Ap. J., 266, 105.

Rickard, L. J., and Blitz, L. 1985, Ap. J. (Letters), 292, L57.

Rowan-Robinson, M. 1980, Ap. J. Supp., 44, 403.

Scoville, N., and Kwan, J. 1976, Ap. J., 206, 718.

Tacconi, L. J., and Young, J. S. 1985, Ap. J., 290, 602.

Telesco, C. M., Decher, R., and Gatley, I. 1985, Ap. J., in press.

Telesco, C. M., and Gatley, I. 1984, Ap. J., 284, 557.

Telesco, C. M., and Harper, D. A. 1980, Ap. J., 235, 293.

Thronson, H. A., and Harper, D. A. 1979, Ap. J., 230, 133.

Thronson, H. A., and Mozurkewich, D. 1986, A. J., submitted.

Thronson, H. A., and Telesco, C. M. 1986, Ap. J., preprint.

Thuan, T., and Martin, G. E. 1981, Ap. J., 247, 823.

Young, J. S., and Scoville, N. Z. 1982, Ap. J., 258, 467.

Young, J. S. Schloerb, F. P., Kenney J. D., and Lord, S. D. 1986, Ap. J., in press.

## FIGURE CAPTIONS

Figure 1 - The distribution of 150 μm emission superimposed upon a photographic image of Hα emission from NGC 4449. In the upper left of the figure a cross with arms 15" long gives the 1σ rms uncertainty in absolute position of the far-infrared contours. The beam size of the 150 μm observations is also shown. Straight lines surrounding the contours are the boundary of the airborne observations. The Hα image was produced from CCD observations obtained at the KPNO #1 0.9 m telescope. A cross near the far-infrared maximum is the location of peak K emission (Table 2). The figure contour drawn is equal to 80. The dashed contour is equal to 10, with the next higher contours equal to 20, 40, and 60.

Figure 2 - Positions sampled by our far-infrared array are shown as dots on the same coordinates as in Figure 1. For clarity, many of the points have been shifted slightly in position in right ascension and the pattern is a consequence in part of field rotation during the observations.

Figure 3 - The infrared spectral energy distribution of NGC 4449. Infrared Astronomical Satellite observations are shown as open circles (Hunter et al. 1986) and our Kuiper Airborne Observatory observations are shown as filled circles. The 1σ rms uncertainty is shown as bars or is equal to the radius of the circle. The lower points refer to flux density values within one detector resolution element at the position of the infrared maximum. A curve of the form $F_\nu \propto \nu B_\nu(25\ K)$ is shown for comparison.

Figure 4 - The distribution of K-band brightness, in magnitudes, from NGC 4449. Peak magnitudes and center positions are listed in Table 1. The boundary of the observations is the light line.

Figure 5 - The distribution of K-band brightness, taken from Figure 4 superimposed upon a blue continuum photograph of NGC 4449 (Canada-France-Hawaii Telescope photograph courtesy of J. Gallagher).

Figure 6 - Scans along the major (above) and minor (below) axes of NGC 4449 at K. The angular distance from the near-infrared peak is shown along the bottom with the corresponding linear radius (assuming a distance to the galaxy of 5.4 Mpc) shown along the top. Two functions were fit by eye to the data and discussed in §IIId. The straight lines through the major axis points are of the form $K(r) \propto r$. Artistic license allowed us to smooth the functions near r = 0. The curved line through the points is a de Vaucouleurs law with $r_0$ = 140" (§IIId).

Figure 7a and 7b - The reliable J = 1 → 0 CO spectra from three positions are shown in (a) and the positions at which four spectra were determined are shown in (b) superimposed upon the same Hα image as used in Figure 1. Offsets from the nuclear position are shown in the upper right of each spectrum. The circles in (b) are equivalent to the beam size of the observations. Table 3 presents the CO line parameters.

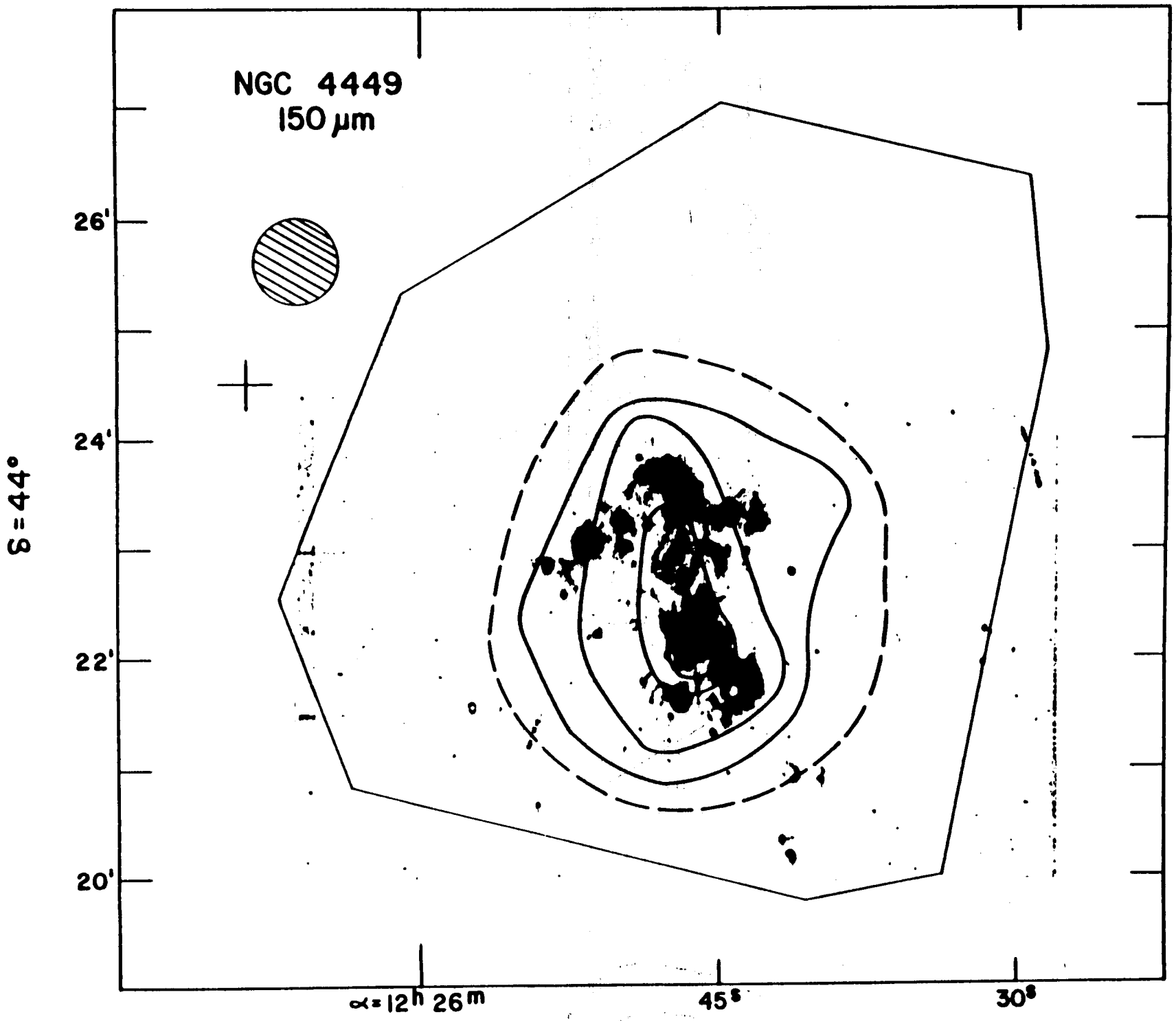
NGC 4449
150 μm
26'
24'
22'
20'
δ = 44°
α = 12h 26m
45s
30s

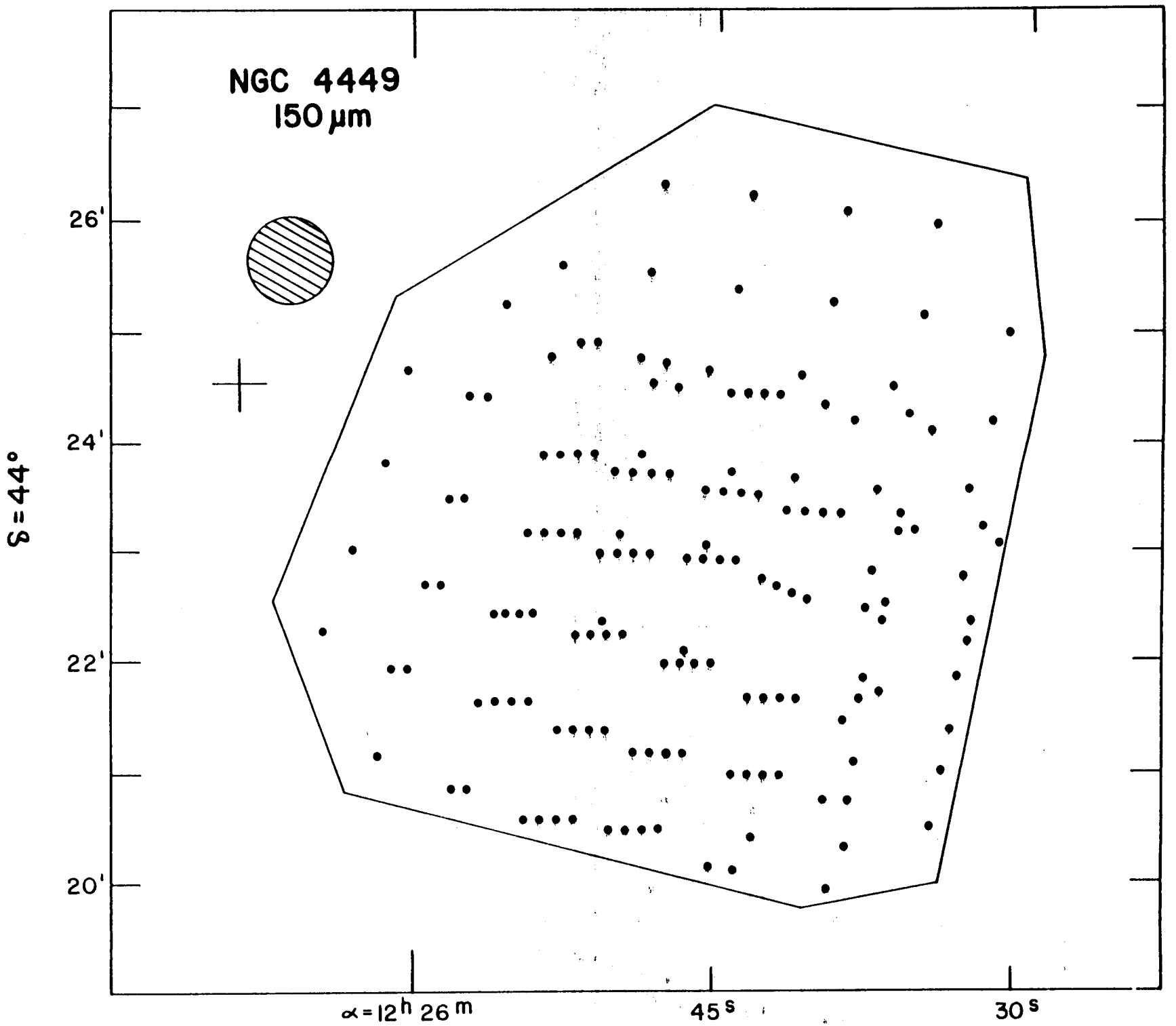
NGC 4449
150 μm
26'
24'
22'
20'
δ = 44°
α = 12h 26m
45s
30s

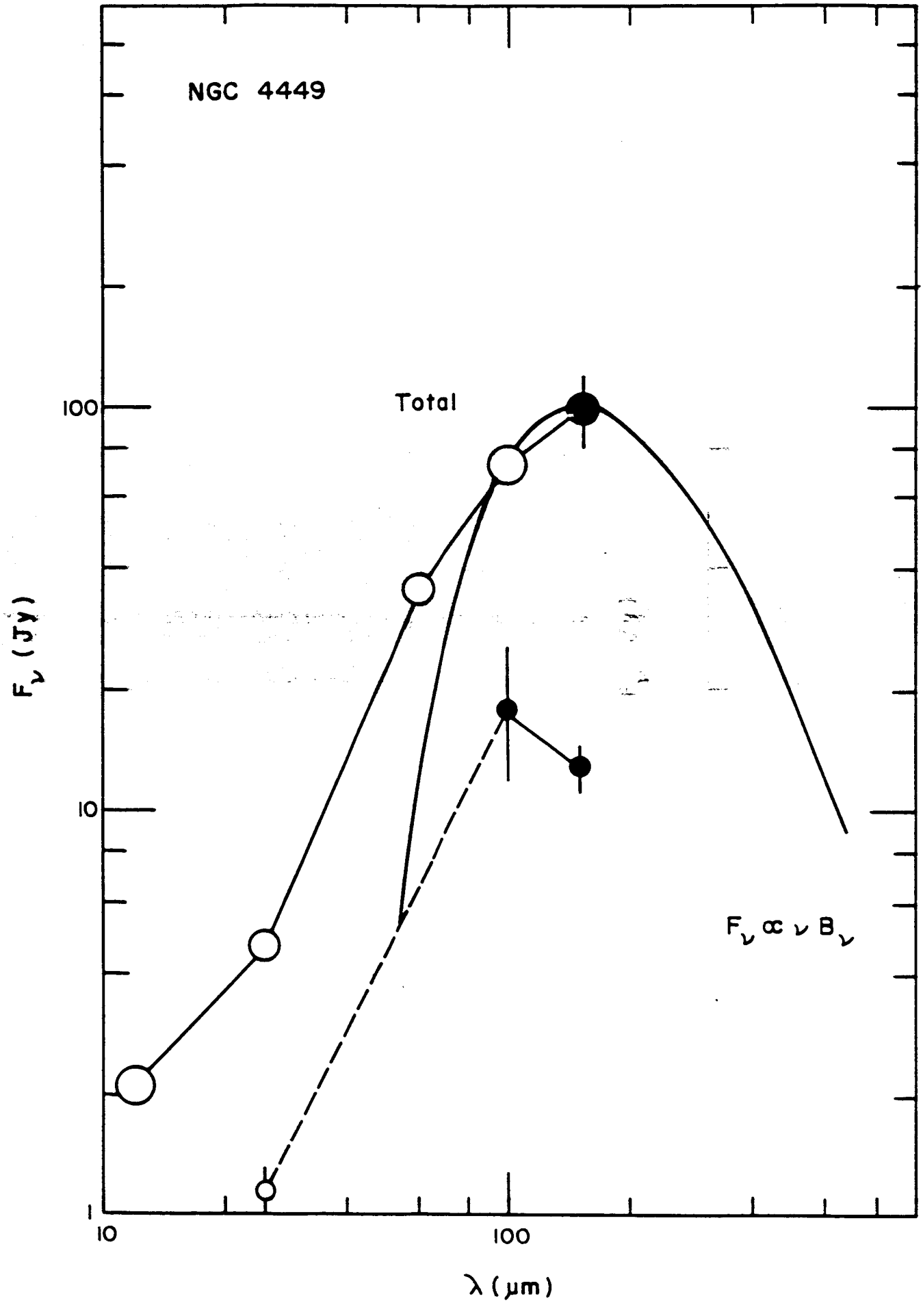
NGC 4449
Total
100
10
1
10
100
$F_\nu$ (Jy)
λ (μm)
$F_\nu \propto \nu B_\nu$

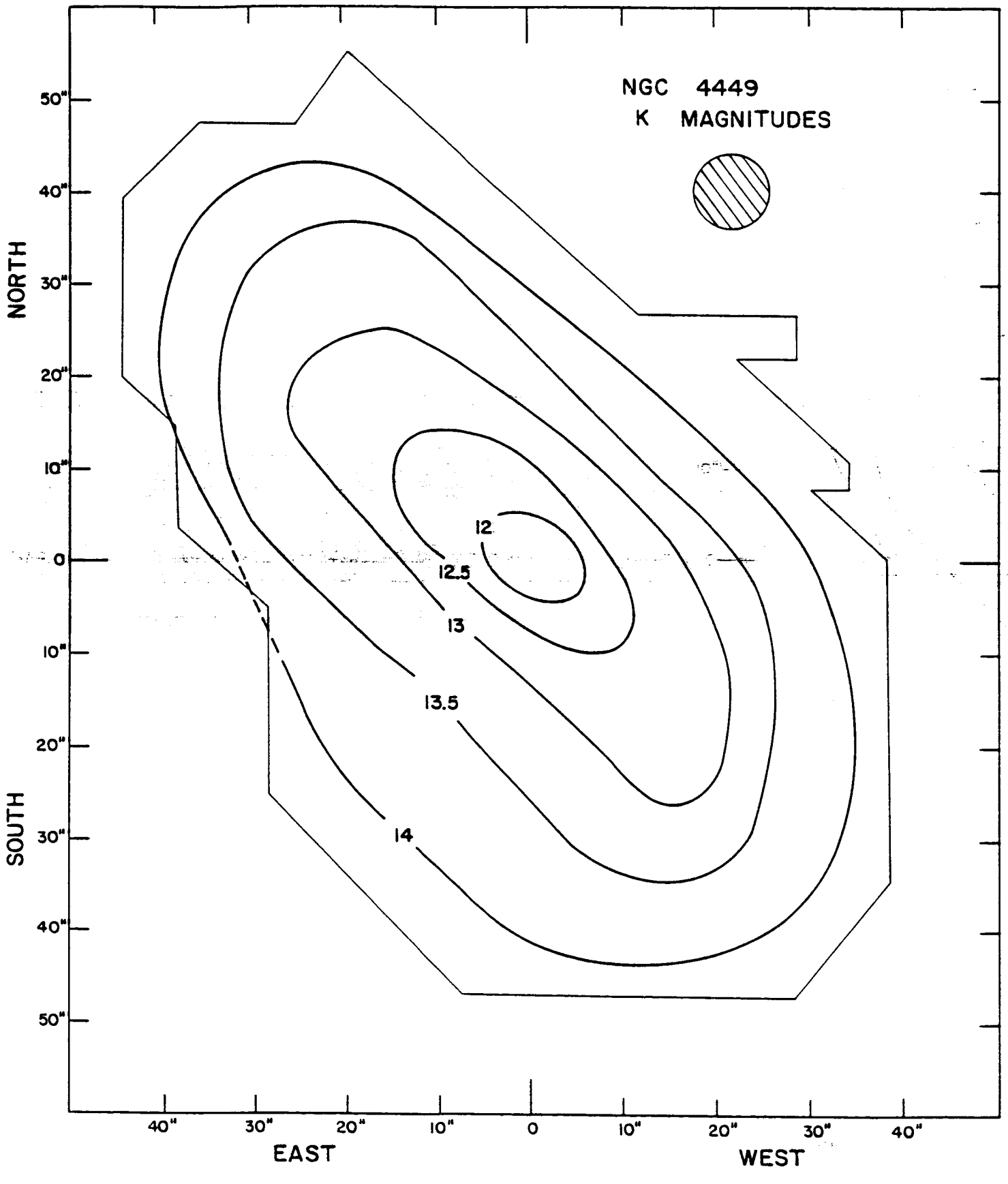
NGC 4449
K MAGNITUDES
NORTH
SOUTH
EAST
WEST
50"
40"
30"
20"
10"
0
10"
20"
30"
40"
50"
12
12.5
13
13.5
14

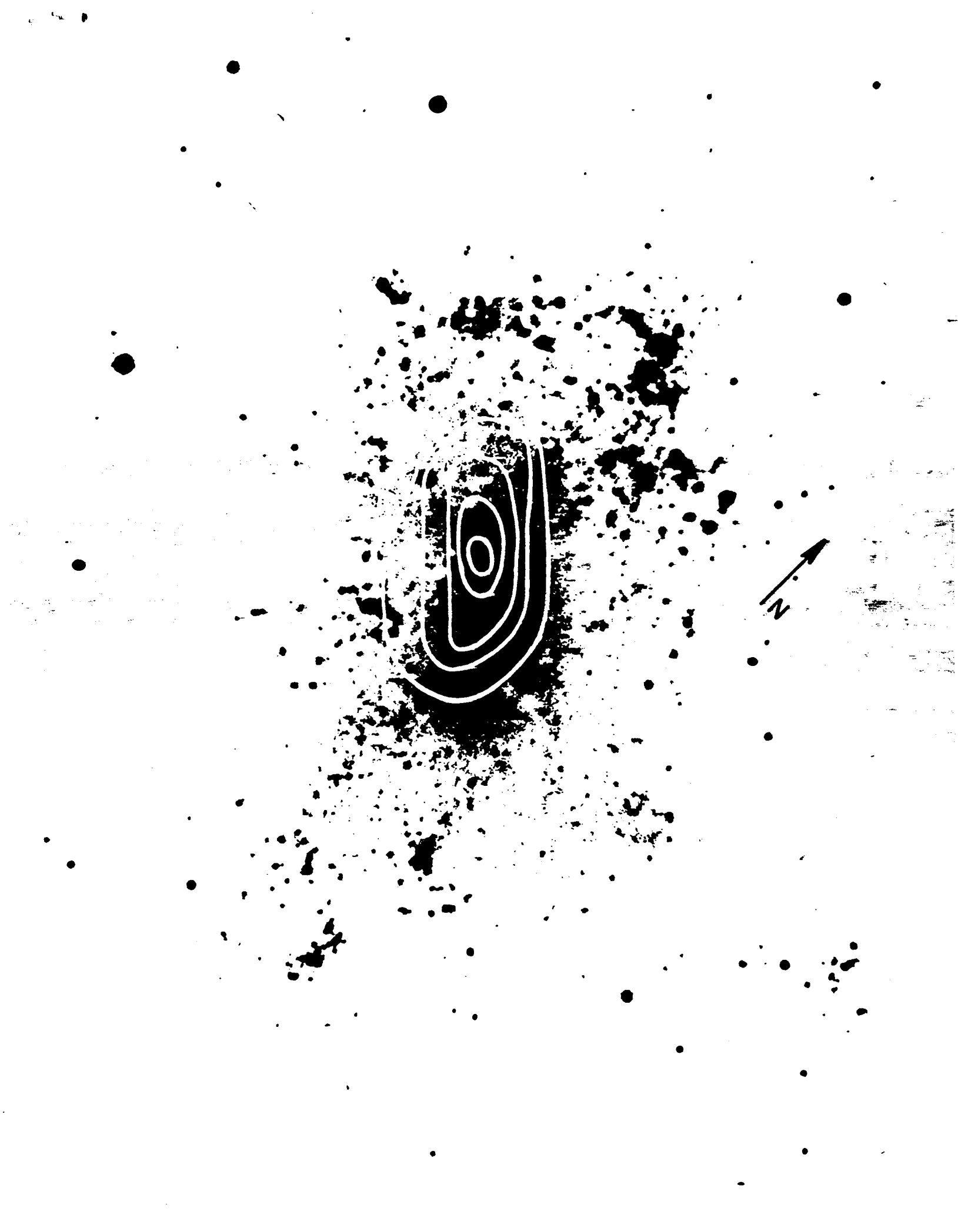
N

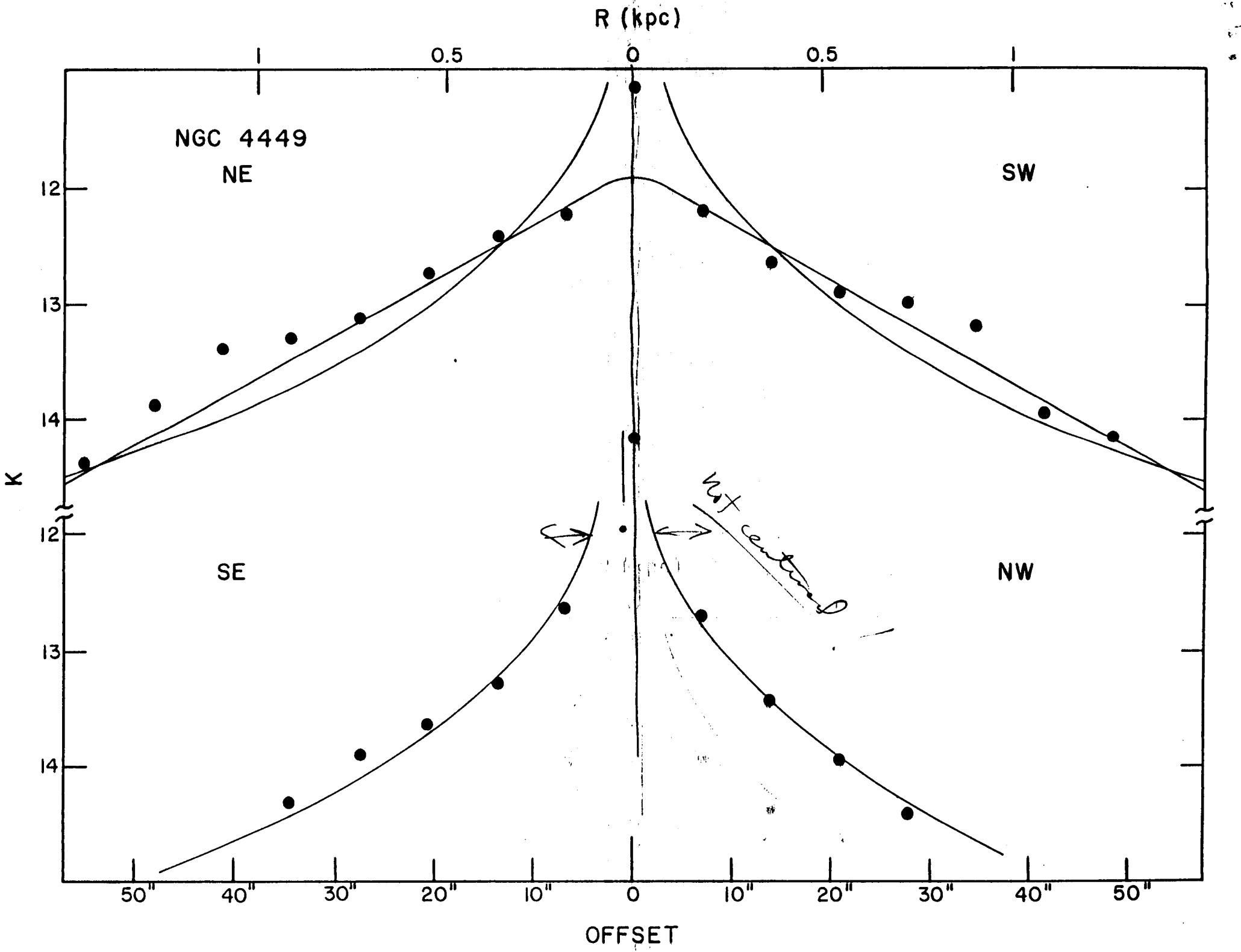
R (kpc)
1
0.5
0
0.5
1
NGC 4449
NE
SW
SE
NW
12
13
14
K
12
13
14
50"
40"
30"
20"
10"
0
10"
20"
30"
40"
50"
OFFSET

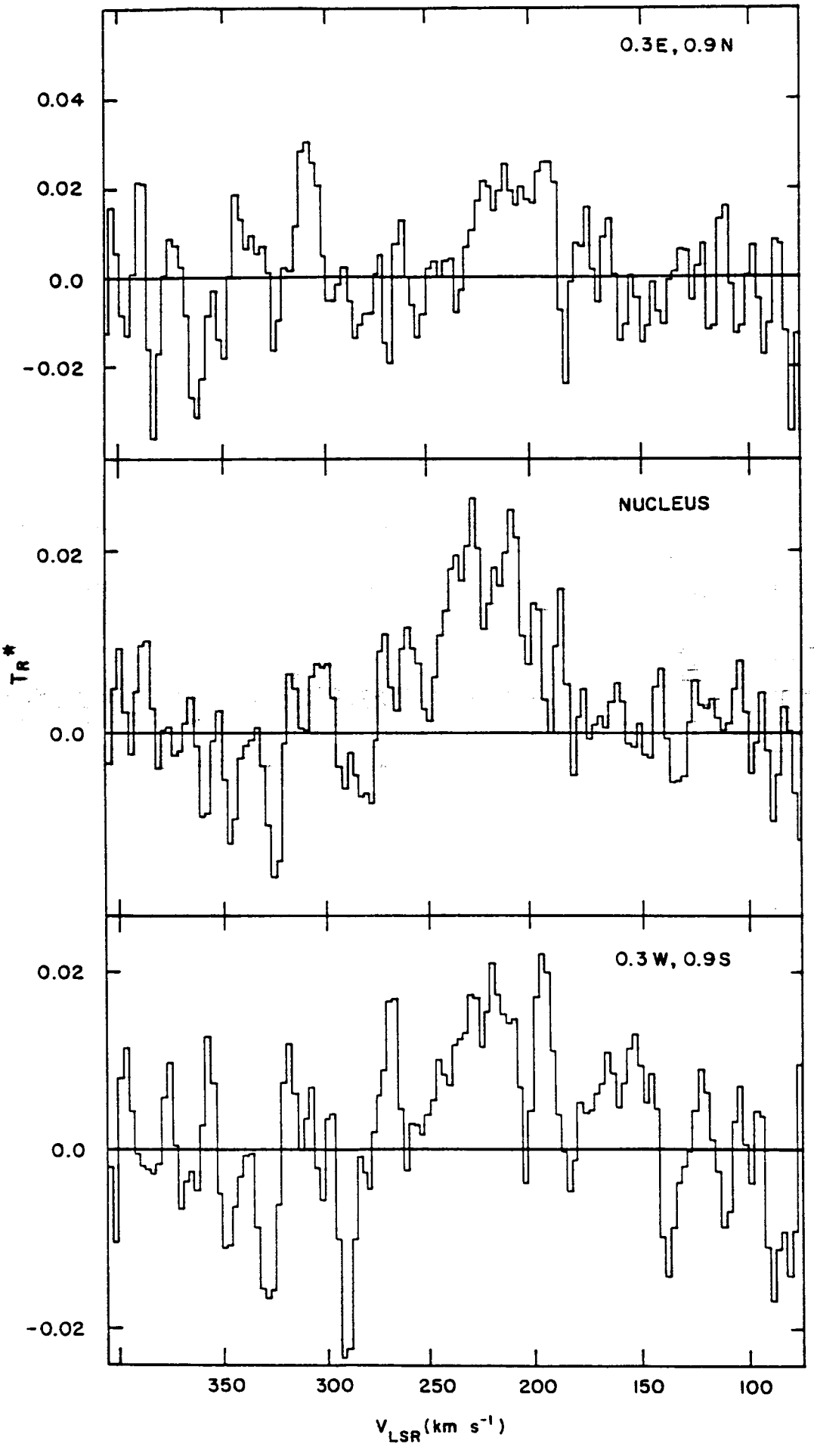
0.3E, 0.9N
NUCLEUS
0.3W, 0.9S
0.04
0.02
0.0
-0.02
$T_R^*$
350
300
250
200
150
100
$V_{LSR}$ (km $s^{-1}$)

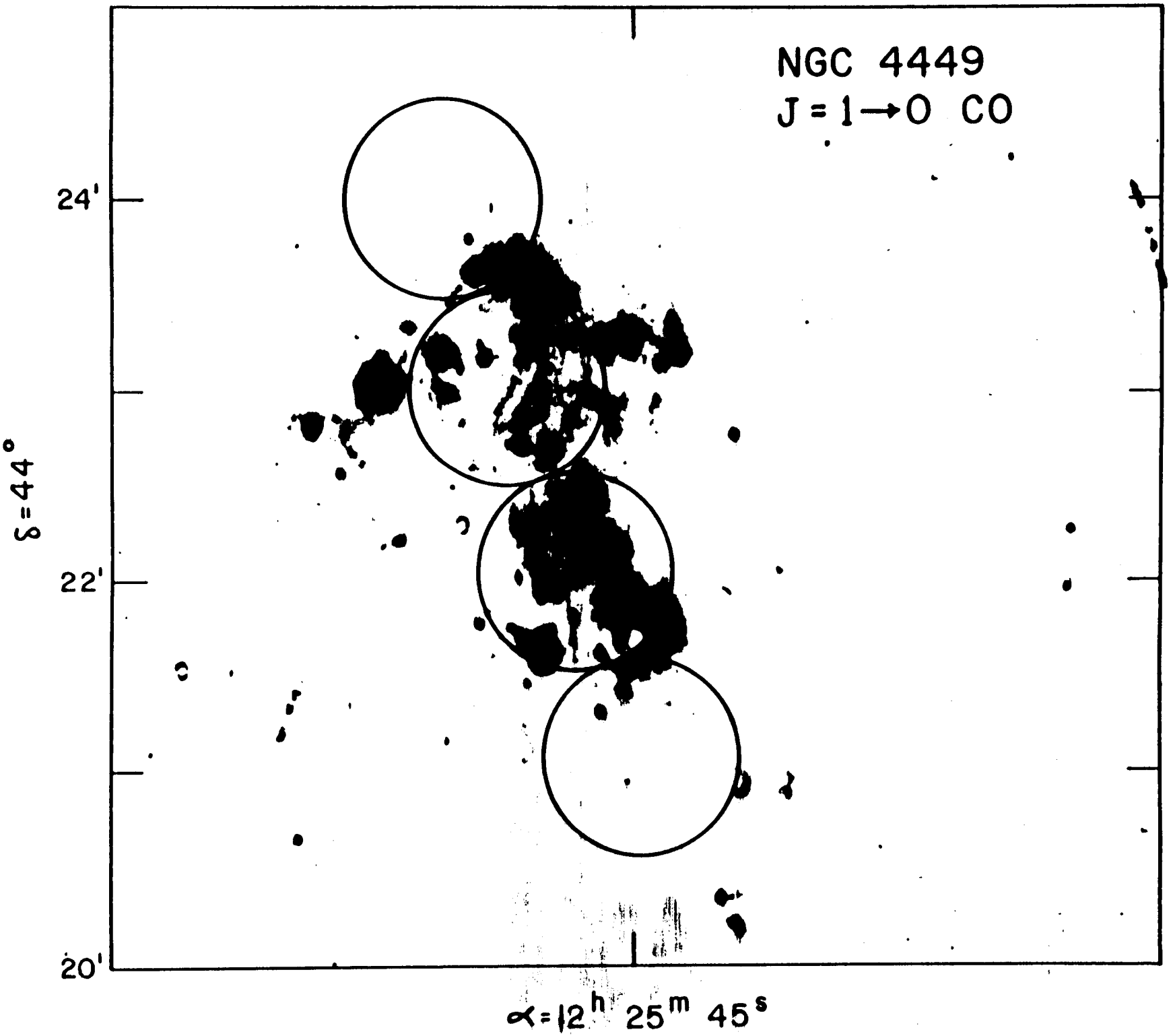
NGC 4449
J = 1→0 CO
24'
22'
20'
δ=44°
α=12h 25m 45s